Research Article

For reprint orders, please contact: reprints@futuremedicine.com

Nanomedicine

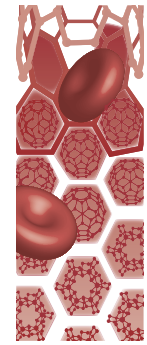

Hampering brain tumor proliferation and migration using peptide nanofiber:si*PLK1*/*MMP2* complexes

Mariarosa Mazza[1], Hassan Ahmad[1], Marilena Hadjidemetriou[1], Giulia Agliardi[1], Omar N. Pathmanaban[3], Andrew T. King[3], Brian W. Bigger[4], Sandra Vranic*,[1,2] & Kostas Kostarelos**,[1,2]

[1]Nanomedicine Lab, Faculty of Biology, Medicine & Health, The University of Manchester, AV Hill Building, Manchester, M13 9PT, UK

[2]National Graphene Institute, The University of Manchester, Booth Street East, Manchester, M13 9PL, UK

[3]Department of Neurosurgery, Salford Royal Hospital, Manchester Academic Health Science Centre, University of Manchester, Manchester, M6 8HD, UK

[4]Stem Cell & Neurotherapies Group, School of Biological Sciences, Faculty of Biology Medicine & Health, Division of Cell Matrix Biology & Regenerative Medicine, University of Manchester, Manchester, M13 9PT, UK

*Author for correspondence: sandra.vranic@manchester.ac.uk

**Author for correspondence: kostas.kostarelos@manchester.ac.uk

Aim: To develop a nonviral tool for the delivery of siRNA to brain tumor cells using peptide nanofibers (PNFs). **Materials & methods:** Uptake of PNFs was evaluated by confocal microscopy and flow cytometry. Gene silencing was determined by RT-qPCR and cell invasion assay. **Results:** PNFs enter phagocytic (BV-2) and nonphagocytic (U-87 MG) cells via endocytosis and passive translocation. si*PLK1* delivered using PNFs reduced the expression of polo-like kinase 1 mRNA and induced cell death in a panel of immortalized and glioblastoma-derived stem cells. Moreover, targeting MMP2 using PNF:si*MMP2* reduced the invasion capacity of U-87 MG cells. We show that stereotactic intra-tumoral administration of PNF:si*PLK1* significantly extends the survival of tumor bearing mice comparing with the untreated tumor bearing animals. **Conclusion:** Our results suggest that this nanomedicine-based RNA interference approach deserves further investigation as a potential brain tumor therapeutic tool.

First draft submitted: 1 August 2019; Accepted for publication: 3 October 2019; Published online: 19 December 2019

Keywords: drug delivery • gene therapy • glioblastoma • nanomedicine • peptide nanofibers • siRNA • U-87 MG

Glioblastoma multiforme (GBM; grade IV glioma brain tumor) is the most common primary malignant brain tumor with a very poor prognosis as less than 5% of the patients survive more than 5 years [1]. The current standard of care is surgical resection followed by chemo-radiotherapy [2]. Despite extensive research and clinical trials, only several drugs are currently approved by US FDA for the treatment of GBM [3,4]. These drugs offer incrementally improved outcome, observed in a minority of patients surviving first 2 years, suggesting that novel approaches are urgently needed to tackle this challenging disease.

RNA interference (RNAi) is a relatively recent technology based on biological process in which biologically active double-stranded siRNA molecules silence gene expression by degrading corresponding mRNA molecules and preventing its translation into functional proteins [5,6]. siRNA-based therapeutics are increasingly explored for the treatment of various types of cancer with the first siRNA-based product (Onpattro®, Alnylam Pharmaceuticals, Inc., MA, USA) being approved in 2018. Nevertheless, there are challenges in translating RNAi-based therapies to the clinic, such as optimizing efficient delivery to tumor cells and into the cytoplasm of targeted cells, maximizing biological activity and overcoming safety concerns [7,8].

Nanoparticle-based medical approaches are currently explored to help overcome the failures of conventional therapies and offer new tools for diagnosis, treatment and intraoperative neuronavigation in order to guide the extent of surgical resection and to minimize injury to the healthy tissue [7,9,10]. We have recently developed a fiber-shaped delivery vector for successful siRNA delivery, peptide nanofibers (PNFs), which are nanostructures

Future Medicine

consisting of self-assembling peptide amphiphiles [11,12]. PNFs are chemically modified biomaterials with an enormous potential in medicine as they can be tailored to address specific needs in different disease settings. By controlling their molecular design, PNFs can encapsulate anticancer drugs, in other words, paclitaxel [13] and camptothecin [14], and act as a tunable release system activated *in situ* by specific enzymes that are highly active in cancer cells [15]. Indeed, PNFs were found to be able to trigger cell death by delivering a cytotoxic component incorporated on the peptide amphiphile sequence [13]. Furthermore, we already demonstrated that complexes of PNF:siRNA can be exploited as a neurosurgical tool to silence genes in deep brain regions, one example being Bcl-2 localized in the subthalamic nucleus [12].

The aim of this study was to develop a nonviral tool for delivery of RNAi therapy to the brain tumor environment, using PNFs as a delivery vector. When choosing a target for RNAi therapy, we wanted to select genes that are highly expressed in tumor cells while not in surrounding healthy brain tissue. One obvious choice was to target cell proliferation and migration, as main distinctive features of tumor versus healthy brain cells. *PLK1* is a gene that controls multiple steps of mitosis and meiosis [16] and is overexpressed in various types of cancers [17], while *MMP2* gene is involved in degradation of extracellular matrix and affects migratory potential of cancer cells [18]. Inhibition of *PLK1* induces cell-cycle arrest leading to cell death [19] and potent inhibitors of *PLK1*, developed in the last decade, are shown to be able to promote tumor regression [20–24]. Currently, *PLK1* inhibitors have entered clinical trial evaluations for the treatment of various types of cancer [25,26]. RNAi therapy based on lipid nanoparticles targeting *PLK1* is also in clinical trial for the treatment of liver cancer (NCT02191878). Specifically relevant to this study, the overexpression of this gene has been reported in brain tumor initiating cells, usually resistant to currently used chemo and radiotherapies. Therefore, PNF:si*PLK1* complexes, we chose to use in this study, could specifically target therapy resistant cells in GBM and may enhance their radio and chemosensitivity [27,28].

We hypothesized that PNFs were able to enter the cells via both endocytosis and passive translocation across the plasma membrane, delivering biologically active siRNA molecules. In the present study, we first aimed to better understand subcellular localization and the mechanism of internalization of PNFs *in vitro*, in GBM relevant cell lines (U-87 MG and BV-2), using confocal microscopy, flow cytometry and imaging flow cytometry. We determined the efficacy of delivered si*PLK1* using reverse-transcription real-time quantitative polymerase chain reaction (RT-qPCR) and immunofluorescence in order to estimate mRNA and protein expression levels. We also followed the downstream cellular effects in a panel of tumor cell lines, glioblastoma-derived stem cell lines and immortalized tumor cells, using cytotoxicity and cell migration assays. Finally, we tested whether the treatment of GBM tumor bearing mice with PNF:si*PLK1* complexes is efficient in extending the survival of tumor bearing animals.

Our results encourage further studies using PNFs as a vector for siRNA delivery in GBM disease models. Localized RNAi therapy that we propose in this study may help overcome some of the problems related to the administration of siRNA molecules via systemic route, such as off-target delivery, low efficacy, imbalanced biodistribution and systemic toxicity.

Experimental

PNF conjugation with VivoTag 680 XL fluorescent probe

VivoTag 680 XL fluorochrome (excitation at 680 nm; emission maximum at 700 nm; Perkin Elmer, Beaconsfield, UK) was reconstituted with 1 ml DMSO, and the 1 mg/ml suspension was made using the freeze-dried peptide and phosphate-buffered saline (PBS). This suspension was transferred into an amber Eppendorf tube to protect it from light. About 50 ml of 1 M sodium bicarbonate and 2 ml of VivoTag 680 XL in DMSO were added. Following steps were the same as described in Mazza *et al.* [12]. The samples were stored at 4°C until needed.

Preparation of PNF:siRNA complexes

PNF:siRNA complexes were prepared as already described by Mazza *et al.* [12]. Briefly, the palmitoyl-GGGAAAKRK peptide amphiphile, custom-made by Peptide Synthetics (Cambridge, UK) as freeze-dried powder, was reconstituted in 5% dextrose (pH = 6.4) to a final concentration 1 mg/ml and filtered through 0.22 µm Millipore membrane filter. The dispersions were subjected to 5 min of probe sonication at 20% of the maximum amplitude alternate pulsed sonication of 20 s each. Complexes were prepared by mixing 0.5 µg of siRNA (AllStars Negative Control siRNA (Qiagen, Manchester, UK, Cat. No.1027281; si*MMP2*, Cat. No.SI02780666, Qiagen; si*PLK1* 5′ → 3′: CCUUGAUGAAGAAGAUCAC, Eurogenetec, Batch No.2101886) at 2.5:1 N/P charge ratio. Complexes were incubated at room temperature for 30 min to allow complete formation.

Cell culture

U-87 MG (ATCC®HTB-14™) and U-87 MG-Luc2 (ATCC®HTB-14-LUC2™) cells were maintained with Dulbecco's minimum essential media supplemented with 10% fetal bovine serum and 1% penicillin/streptomycin. BV-2 cells were maintained with RPMI 1640 media supplemented with 10% fetal bovine serum and 1% penicillin/streptomycin.

Human brain tumor stem cells

Patient cell line derivation was in accordance with Pollard *et al.* [29]. Dissociated tumor cells were cultured in neurobasal medium supplemented with N2, B27, EGF and FGF-2 (20 ng/ml). Laminin was added to the media (25 ng/ml final concentration) to improve cellular adherence. Cells were maintained in a standard tissue culture incubator (37°C; 5% CO_2) and media and growth factors replenished regularly until cells reached 90% confluence. Neurosphere forming ability was tested by passaging in supplemented neurobasal medium in the absence of laminin. Spheroids typically formed within 24 h.

Bright field imaging of the cells

Bright field microscopy was used to assess changes in confluency and morphology of U-87 MG-Luc2 cells after treatment with PNF:si*PLK1*. Cells were seeded in 96 well plates (2000 cells/well). After 24 h, cells were treated with PNF:si*PLK1*, lipo:si*PLK1* and PNF:siNEG, using 80 nM final concentration of si*PLK1* and siNEG. Cells treated with si*PLK1*, siNEG, PNFs only and Lipofectamine:siNEG and Lipofectamine:si*PLK1* were used as controls. Cells were incubated at 37°C in 5% CO_2, and after 4 h serum was added to obtain 10% final serum concentration. Cells were then incubated at 37°C in 5% CO_2 for the following 20 or 44 h and bright field images were captured using Olympus microscope.

Confocal microscopy

Detection of siRNA subcellular localization

AlexaFluor®546-labeled noncoding siRNA was used to form PNF:siRNA to assess the internalization mechanism of PNF:siRNA complexes by U-87 MG-Luc2 cells. Cells were seeded onto 24-well glass bottom plate (2000 cells/well). After 1 h, endosomes were stained with 100 µg/ml pHrodo™ Green Dextran (Life Technologies, Manchester, UK), diluted in cell culture medium, for 10 min at 37°C in 5% CO_2. After that, cells were washed with cell culture medium, treated with PNF:siRNA and Lipofectamine:siRNA complexes at a final concentration of siRNA 80 nM and incubated for 1 h at 37°C in 5% CO_2. Cells treated with Lipofectamine, PNFs and AlexaFluor®546-labeled noncoding siRNA (80 nM) were used as controls. Images were collected on Leica TCS SP5 AOBS inverted confocal microscope using a 63 ×/1.4 oil objective. The confocal settings were as follows: pinhole 1.88 airy unit, scan speed 400 Hz bidirectional, format 512 × 512. Images were collected using the following laser lines: 514 (15%), 561 (19%). To eliminate the cross-talk between the channels, images were collected sequentially.

Immunolabeling

U-87 MG-Luc2 cells were seeded onto 8-well glass slide (6000 cells/well). After 24 h, cells were treated with PNF:si*PLK1*, Lipo:si*PLK1* and PNF:siNEG, using 80 nM final concentration of si*PLK1* and siNEG. Naive cells, cells treated with si*PLK1*, siNEG and cells treated with PNFs only were used as controls. After 30 min, 4 and 24 h of incubation at 37°C in 5% CO_2, cells were fixed by methanol, precooled at -20°C. Immunolabeling was performed as described in Mazza *et al.* [12]. Primary antibody we used was PLK1 antibody (Cell signaling, UK #4535), at 1:50 dilution in 0.1% Triton-2% bovine serum albumin (BSA)-PBS for 2 h at room temperature (RT) in a humidified chamber. Secondary antibody was Cy3-conjugated goat anti-rabbit IgG (Jackson Immunoresearch, Ely, UK) using 1:125 dilution in 5% normal goat serum (NGS)-0.1% Triton-PBS. Samples were analyzed under fluorescence microscopy (AX10 Zeiss). Specificity of the secondary antibody was also verified, by performing labeling using secondary antibody only. For 24-h time point, serum was added after 4 h of incubation to each well to obtain final serum concentration of 10% and cells were incubated at 37°C in 5% CO_2 for the following 20 h before immunofluorescence assay.

Imaging flow cytometry

BV-2 and U-87 MG cells were treated after reaching 80% confluence with 25 and 10 µg/ml PNFs respectively at 37 or 4°C, for 30 min or 3 h. Cells were collected and prepared for analysis as already described by Vranic

et al. [30–32]. Briefly, at the end of the exposure to PNFs, cells were washed with PBS and harvested using Trypsin-EDTA. Cell suspensions were centrifuged for 5 min at 1500 rpm at 4°C and the pellets were fixed in 500 µl of 4% para-formaldehyde (Thermo Fisher Scientific, Manchester, UK). After 20 min of incubation in PFA at the room temperature, cells were rinsed three-times in PBS and finally diluted in 60 µl PBS. At least 2500 cells were analyzed using Amnis® ImageStream® MKII (Millipore, Watford, UK) and Inspire™ system software (Amnis, UK). Camera magnification was 60×, 642 nm excitation laser was set at 75 mW. All images were acquired with the normal depth of field, providing a cross-sectional image of the cell with a 2.5 µm depth of focus. A mask representing the whole cell was defined by the bright-field image, and an internal mask was defined by eroding the whole cell mask by 6 pixels (equivalent to 3 µm, as the size of 1 pixel was 0.5 µm) in order to eliminate the fluorescent signal coming from the PNFs attached to the cell surface, thus measuring only the internalized part. The results were analyzed using IDEAS 6.1 software (Amnis). Values of the internalization score (IS) and mean fluorescence intensity (MFI) were calculated for at least 800 cells per sample. Each condition was run in duplicates.

Inhibition of endocytosis using pharmacological inhibitors

Cellular uptake studies were carried out in U-87 MG and BV-2 cell lines. Both cell lines were incubated with PNFs for 30 min and 3 h. All inhibitors were obtained from (Sigma-Aldrich, Dorset, UK). All pharmacological inhibitors were initially screened for working concentrations that did not affect cellular morphology and viability. All experiments were done in serum free media. To inhibit energy-dependent endocytosis cells were treated with Sodium azide (5 mM for U-87 MG, 10 mM for BV-2 cells) or incubated at 4°C. Clathrin-mediated endocytosis was inhibited with the use of chlorpromazine (1 µg/ml for U-87 MG, 10 µg/ml for BV-2 cells). Caveolae-mediated endocytosis was inhibited with genistein (20 µM for both cell lines). Dynasore (80 µM for both cell lines) was used to inhibit both clathrin and caveolae-mediated endocytosis, while macropinocytosis was disrupted with amiloride (40 µM for both cell lines). Cells were pretreated with inhibitors for 30 min and then treated with PNFs in the presence of inhibitors for the following 30 min or 3 h.

Flow cytometry

After treatment of the cells with PNFs in the presence or absence of pharmacological inhibitors at indicated time points, cells were harvested using Trypsin-EDTA. The activity of trypsin was stopped using 10% fetal bovine serum (FBS). The BD FACSverse (Becton, Dickinson and Company, NJ, USA) was used to analyze the samples. Threshold values were kept consistent throughout analysis of all samples. All samples were run in triplicates and an average of the mean fluorescence values was calculated to give the MFI of each treatment condition.

RT-qPCR

U-87 MG cells were seeded in sixwell plates and allowed to reach 60–80% confluence prior treatment. Cells were transfected in serum free media using PNF:si*PLK1*, PNFs, si*PLK1*, siNEG and PNF:siNEG, using 80 nM final concentration of si*PLK1* and siNEG. All experiments were performed in triplicates. Total RNA was extracted with Macherey–Nagel kit according to the manufacturer's instructions. RT-qPCR was performed as already described in Guo *et al.* [33]. The statistical significance of the results was evaluated using the One-way ANOVA analysis followed by analysis with the Dunnett's test with 95% CI.

Lactate dehydrogenase cytotoxicity assay

Cells were seeded in 96-well plates and treated with increasing concentrations of PNFs for 24 h. Lactate dehydrogenase (LDH) released due to cell lysis reflects cell death induced by the treatment. A 50 µl of supernatant was transferred to a new 96-well plate, mixed with 50 µl of LDH substrate mix (CytoTox 96® nonradioactive cytotoxicity assay, Promega, UK) and left to react for 45 min at room temperature, after which 50 µl of stop solution was added. The absorbance was read at 490 nm using a spectrophotometer plate reader (FLUOstar Omega, BMG Labtech, Ayelsbury, UK).

Effect of PNF:si*PLK1* in U-87 MG orthotopic GBM model

All experiments were performed in accordance with the approved recommendations and policies of the UK Home Office (Animal Scientific Procedures Act 1986, UK). Athymic nude mice (4-week old, Harlan, UK) were anesthetized by inhalation of isoflurane and administered buprenorphine (0.05 mg/kg) prior to the surgery. Mice were implanted with 2×10^5 U-87 MG-Luc2 cells in the right striatum: a burrhole is made 0.1 mm posterior to

bregma and 2.3 mm to the right of the midline, the syringe is moved down into the position at depth of 3 mm and kept in place for 3 min. The needle is withdrawn 0.4 mm to a total depth of 2.6 mm below the surface of the brain, creating a small pocket where the cells are infused over 3 min. Animals (n = 5) were intratumorally, stereotactically injected with PNF:si*PLK1* (PNF = 414 ng; si*PLK1* = 174.5 ng) complexes 14 days after tumor implantation while control groups received PNFs only, si*PLK1* only or remained untreated (n = 4). Only one group of animals received a second administration of PNF:si*PLK1*, 21 days after tumor implantation. Tumor progression was measured before and after treatment using Bioluminiscence Imaging IVIS Lumina II camera after animals were subcutaneously injected with D-luciferin in PBS (15 mg/kg).

Results

Internalization & subcellular localization of PNF:siRNA complexes

Intracellular localization of PNFs

PNFs used in this study are composed of three basic amino acids (KRK) and form complexes with siRNA through electrostatic interactions, as we have already reported [11]. The polar head of the peptide amphiphile we used in this study is made of three basic amino acids (KRK), conferring a net positive charge at physiologic pH, which makes binding of the siRNA molecule electrostatically favorable. PNFs we used have been thoroughly characterized in our previous publications [11,12]. In 2015, we demonstrated that PNFs started forming complexes with siRNA already at 2.5:1 (PNF:siRNA) ratio, while full complexation occurred at 7.5:1 mass ratio [12]. Overall charge of complexes was also evaluated, indicating that surface charge of PNFs shifted from positive (30.8 ± 2.06 mV) to more negative values (-13.1 ± 3.04 mV) upon complexation with siRNA at 7.5:1 (PNF:siRNA) ratio in water [12]. As shown in Figure 1A, complexation of siRNA molecules with PNFs results in condensation of siRNA around the fiber. Transmission electron microscopy (TEM) micrographs reported in Mazza *et al.* support this finding [12].

As a first step in investigating the ability of PNFs to act as a vector for intracellular siRNA delivery, we studied the subcellular localization of PNF:siRNA complexes in human glioblastoma cell line (U-87 MG-Luc2) using confocal laser scanning microscopy. To study subcellular localization of PNF:siRNA complexes, we labeled acidified intracellular vesicles (endosomes and lysosomes) with pHrodo™ Green Dextran, a dye that confers green fluorescent signal to the vesicles as their pH decreases from neutral to acidic. A noncoding, fluorescently labeled siRNA (siRNA-AlexaFluor®546) was used in this experiment. U-87 MG-Luc2 cells were transfected with PNF:siRNA-AlexaFluor®546 complexes and live cell confocal laser scanning microscopy was used to observe internalization and kinetics of the uptake. At 1 h post-transfection, red fluorescent signal coming from the siRNA-AlexaFluor®546 was localized in the periphery of the cell and around endosomes (Figure 1B, insets 1 & 2). This result suggests that siRNA was delivered intracellularly using PNFs as a vector and localized in the cytosolic compartment of the cells as well as on the plasma membrane of the cells.

Semi-quantification of PNFs uptake

In order to better characterize the uptake of PNFs *in vitro*, we used two cell lines relevant for GBM and tumor microenvironment: nonphagocytic, glioblastoma (U-87 MG) and phagocytic, microglia (BV-2) cell lines. Imaging flow cytometry was used to image and semi-quantify the uptake of fluorescently labeled PNFs by the cells. Figures 2 & 3 show the uptake of PNFs by U-87 MG and BV-2 cells treated for 30 min or 3 h with fluorescently labeled PNFs at 4 or 37°C.

Looking at the images first, treatment of the cells at 4°C clearly shows that PNFs are mainly localized on the cell surface (BF/PNF overlay), whereas after treatment at 37°C, they were found inside the cells (punctual as well as diffused signal), but also on the cell surface for both cell lines. Second, it was possible to semi-quantify the uptake by defining a mask representing the whole cell as well as the second, internal, mask by eroding the whole cell mask to take into account inside of the cell only. This enables elimination of the fluorescent signal coming from the PNFs attached to the cell surface and thus quantifies only internalized PNFs. Comparison of the fluorescence detected inside the eroded mask with the whole cell fluorescence defines the IS. A positive value of IS corresponds to a cell with mostly internalized PNFs, whereas a negative IS corresponds to a cell with mostly surface-associated PNFs. Mean IS values in the Figures 2B & 3B show that most cells treated at 4°C had a negative IS indicating adsorption of PNFs on the cell surface. For the cells treated at 37°C, the IS was positive, showing that the majority of the cells had internalized PNFs confirming the observations on the corresponding images in 3A and thus validating the applied mask.

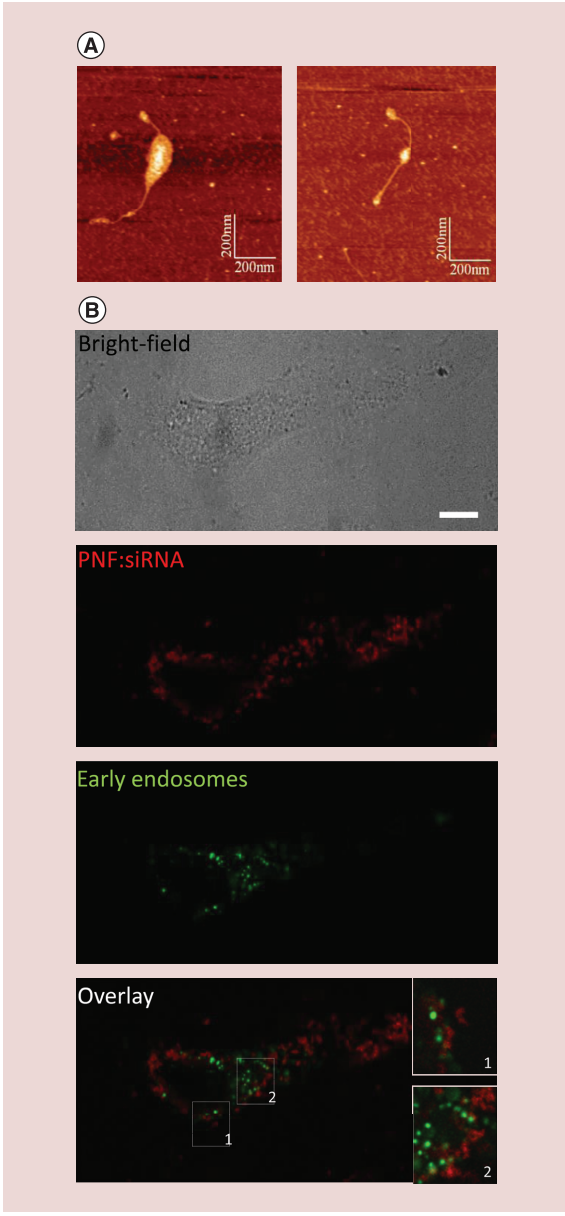

Figure 1. Internalization of peptide nanofiber:siRNA complexes by U-87 MG-Luc2 cells. (A) Atomic force microscopy images of peptide nanofiber (PNF):siRNA complexes. **(B)** Live cell confocal imaging of U-87 MG-Luc2 cells treated with PNF:siRNA-AlexaFluor®546 complexes (red), stained with early endosomal marker pHrodo™ Green (green). 1 h after incubation, PNF:siRNA-AlexaFluor®546 complexes are detected around endosomes. Insets (1–2) show higher magnification of the areas marked with rectangles; scale bar = 10 μm.

After validation of the mask, we calculated MFI coming from the PNFs inside the mask and showed that the uptake of PNFs by both cell types was a time- and temperature-dependent process. As shown in Figures 2C & 3C, the MFI values of the treated cells increased with time of the exposure and were depended on the temperature. Incubation at 4°C blocked the uptake significantly for U-87 MG and almost completely for the BV-2 cell line suggesting that passive penetration of the PNFs across the plasma membrane was occurring in U-87 MG cell line, and to a lesser extent in BV-2 cells.

Endocytic mechanism

To dissect the endocytic mechanism used by the two cell lines, we studied the uptake of fluorescently labeled PNFs by flow cytometry, after treatment with inhibitors of different endocytic pathways. All pharmacological inhibitors were initially screened for working concentrations that did not affect cellular morphology and viability.

In order to inhibit energy-dependent uptake pathways, cells were pre-incubated at 4°C or treated with sodium azide. When U-87 MG cells were incubated with PNFs at 4°C, there was a 55% ± 9.77 reduction in the uptake after 30 min and 76% ± 17.9 reduction in uptake after 3 h of treatment (Figure 4A). In BV-2 cells incubated at 4°C, we found 81% ± 2.9 reduction in the uptake after 30 min and 94% ± 0.15 reduction in the uptake

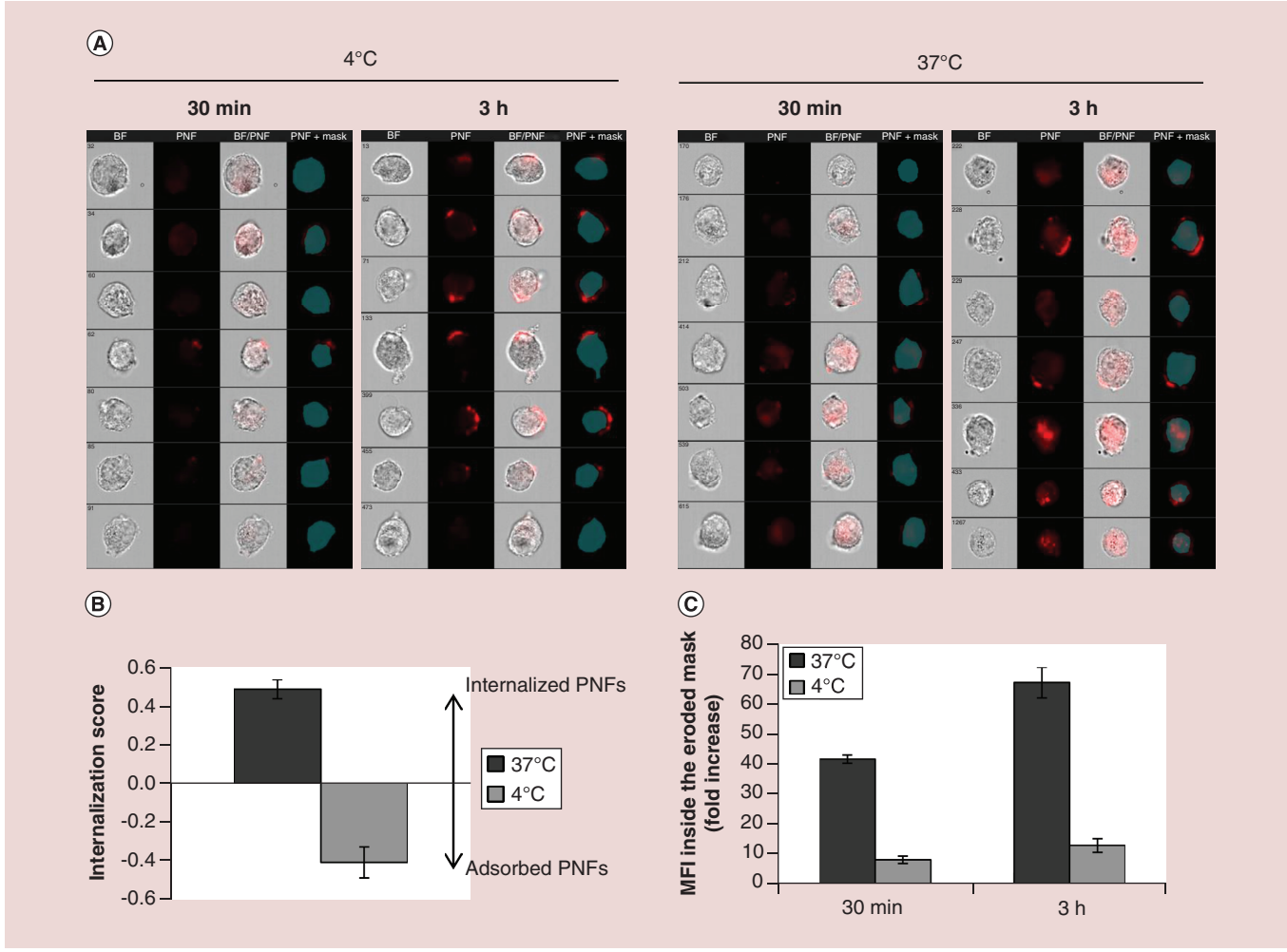

Figure 2. Semi-quantification of the uptake of fluorescently labeled peptide nanofibers by U-87 MG cells using imaging flow cytometry. (A) Representative images of the cells treated with PNFs (conjugated with VivoTag 680 XL fluorescent probe) for 30 min or 3 h at 37 or 4°C captured using imaging flow cytometry. In each panel, first column shows bright-field (BF) images of the cells, second column shows fluorescence of the PNFs (PNF), third column shows the PNFs fluorescence merged with the BF image of the cells (BF/PNF) and fourth column shows the overlay of the applied mask and the PNF fluorescence (PNF+Mask). **(B)** Internalization score calculated by Amnis IDEAS® software: values of internalization score of the cells treated with PNFs for 3 h at 37 or 4°C and **(C)** corresponding fold increase of the MFI values inside the mask normalized to the values of untreated cells at indicated time points and temperatures.
MFI: Mean fluorescence intensity; PNF: Peptide nanofiber.

after 3 h of treatment (Figure 5A). When sodium azide was used to inhibit energy-dependent processes within the cell, in U-87 MG cells after 30 min of treatment a similar reduction of the uptake was observed as when the cells were exposed to 4°C (56% ± 4.75 inhibition), while after 3 h the reduction of the uptake reached 64% ± 6.10 (Figure 4B). The effect was even more pronounced in BV-2 cells as 75% ± 3.67 and 83% ± 3.95 inhibition of the uptake were observed at 30 min and 3 h of treatment, respectively (Figure 5B).

To inhibit clathrin-mediated endocytosis, cells were treated with chlorpromazine and dynasore inhibitors. Treatment with chlorpromazine in U-87 MG cells led to a 49% ± 5.41 and 54% ± 14.35 decrease of PNF uptake at 30 min and 3 h of treatment, respectively (Figure 4C). Pretreatment with dynasore induced 81% ± 6.21 reduction of PNFs uptake at 30 min, and a reduction of 89% ± 2.80 PNFs uptake at 3-h time point (Figure 4D). Chlorpromazine treatment, in BV-2 cells, resulted in a 68% ± 2.88 internalization reduction at 30 min, however the uptake of PNFs increased at the 3-h time point as only a 40% ± 8.48 inhibition was observed (Figure 5C). Pretreatment with dynasore induced a drastic internalization reduction of 92% ± 5.29 at 30 min that decreased to 87% ± 3.67 at 3 h (Figure 5D).

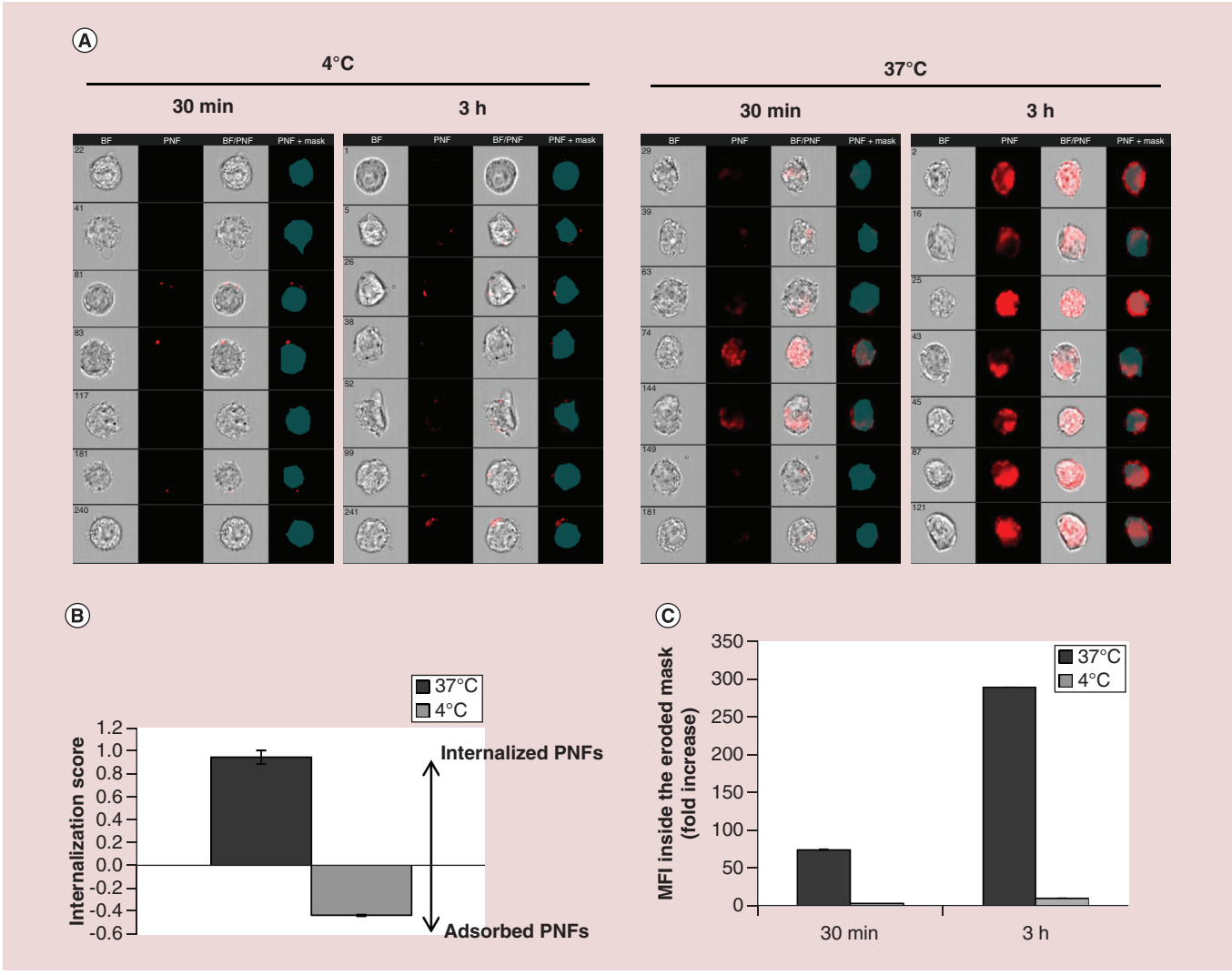

Figure 3. Semi-quantification of the uptake of fluorescently labeled peptide nanofibers by BV-2 cells using imaging flow cytometry. (A) Representative images of BV-2 cells treated with PNFs (conjugated with VivoTag 680 XL fluorescent probe) for 30 min or 3 h at 37 or 4°C captured using imaging flow cytometry. In each panel, first column shows bright-field (BF) images of the cells, second column shows the fluorescence of PNFs (PNF), third column shows PNFs fluorescence merged with the BF image of the cells (BF/PNF) and fourth column shows the overlay of the applied mask and PNF fluorescence (PNF+Mask). **(B)** Internalization score calculated by Amnis IDEAS® software: values of internalization score of the cells treated with PNFs for 3 h at 37°C or 4°C, and **(C)** corresponding fold increase of the MFI values inside the mask normalized to the values of untreated cells at indicated time points and temperatures.
MFI: Mean fluorescence intensity; PNF: Peptide nanofiber.

Caveolae-mediated endocytosis was investigated using Genistein. Pretreatment of U-87 MG cells with Genistein resulted in the reduction of internalization of PNFs up to 68% ± 2.5 after 30 min of incubation, however after 3 h, this decreased to only 19% ± 3.91 (Figure 4E). Genistein treatment of BV-2 cells resulted in the reduction of internalization of PNFs of 55% ± 1.50 at 30 min and 53% ± 8.93 at 3 h (Figure 5E).

Macropinocytotic pathway was inhibited using Amiloride, a Na^+/K^+ exchange blocker. Pretreatment of U-87 MG with Amiloride resulted in a reduction of internalization of PNFs of 80% ± 1.03 after 30 min of incubation, however after 3 h, this decreased to only 7% ± 6.14, an effect similar to what was observed with Genistein (Figure 4F). Amiloride treatment on BV-2 cells resulted in a reduction of internalization of PNFs of 61% ± 2.54 at 30 min and 48% ± 2.77 at 3 h (Figure 5E).

At last, phagocytic pathway was inhibited using Cytochalasin B in BV-2 cells, as this is a phagocytic murine microglial cell line. Flow cytometry analysis revealed a reduction of internalization of 74% ± 2.99 after 30-min incubation and 82% ± 0.19 after 3 h (Figure 5G).

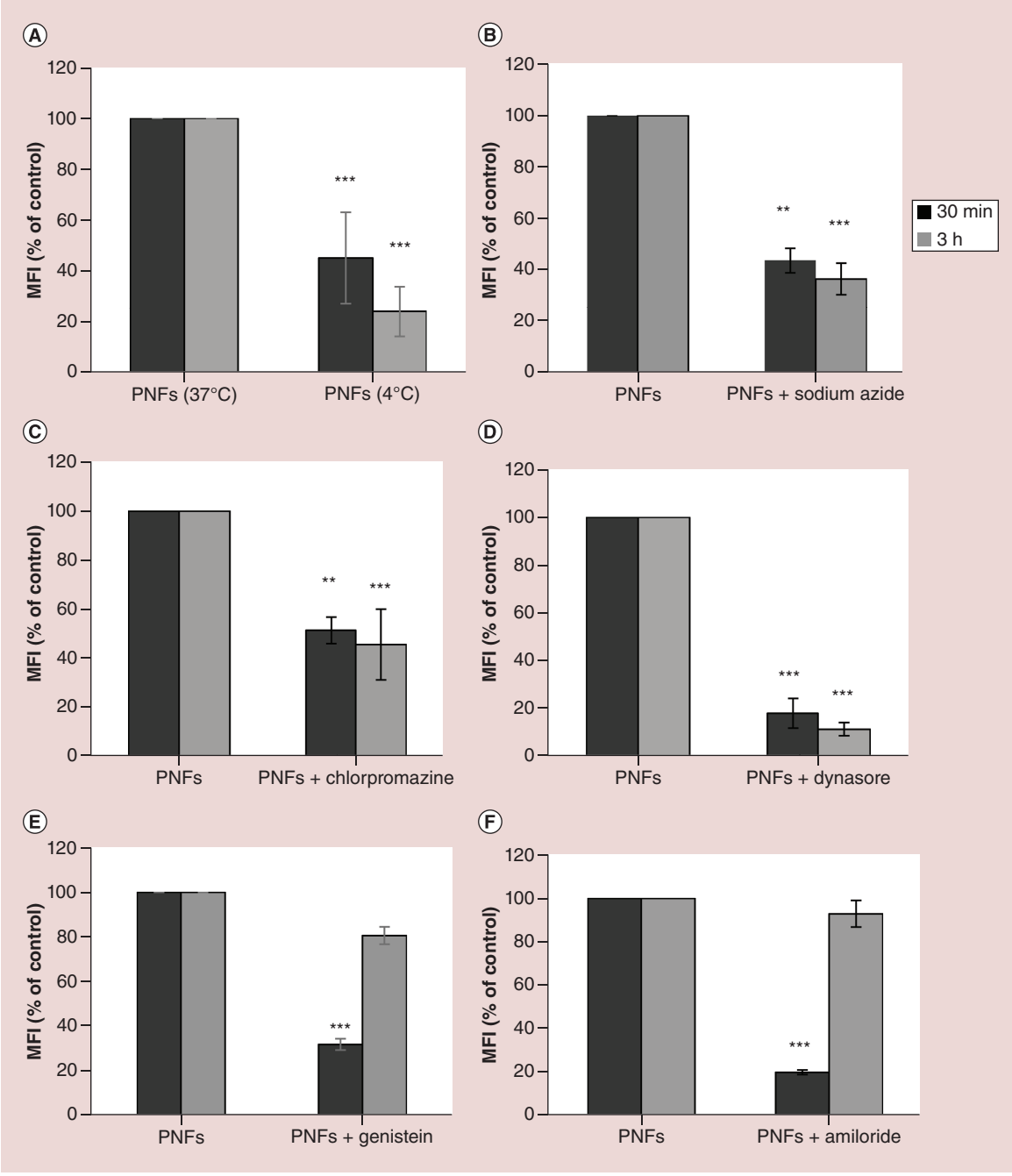

Figure 4. The mechanism of endocytosis of fluorescently labeled peptide nanofibers in U-87 MG cells, studied by flow cytometry upon inhibition of different endocytic pathways using pharmacological inhibitors. (A & B) Inhibition of energy-dependent uptake pathways, using either incubation of the cells with PNFs at 4°C or in the presence of sodium azide (5 mM). **(C & D)** Inhibition of clathrin-mediated endocytic pathway using either chlorpromazine (1 μg/ml) or dynasore (80 μM). **(E)** Inhibition of caveolae-mediated endocytic pathway using genistein (20 μM). **(F)** Inhibition of macropinocytosis using amiloride (40 μM). Mean values ± standard deviation were obtained from three independent experiments. One-way ANOVA, followed by Tukey's post-analysis test were used to determine the statistical significance of the data obtained with the different inhibitors compared with the cells treated with PNFs only (**$p < 0.01$; ***$p < 0.005$).
MFI: Mean fluorescence intensity; PNF: Peptide nanofiber.

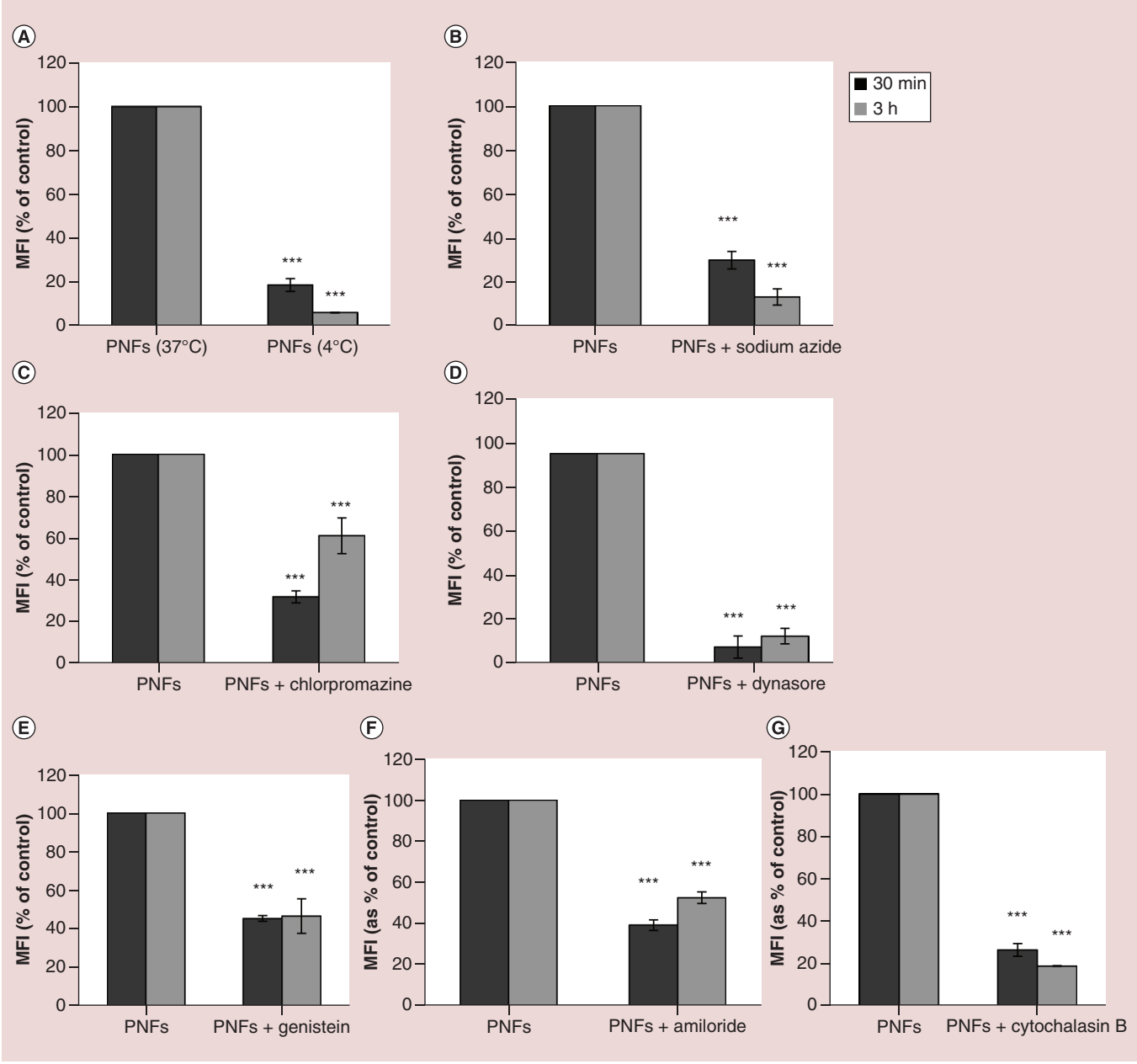

Figure 5. The mechanism of endocytosis of fluorescently labeled peptide nanofibers in BV-2 cells, studied by flow cytometry upon inhibition of different endocytic pathways using pharmacological inhibitors. (A & B) Inhibition of energy-dependent uptake pathways, using either incubation of the cells with PNFs at 4°C or in the presence of sodium azide (20 mM). **(C & D)** Inhibition of clathrin-mediated endocytic pathway using either chlorpromazine (10 μg/ml) or dynasore (80 μM). **(E)** Inhibition of caveolae-mediated endocytic pathway using genistein (20 μM). **(F)** Inhibition of macropinocytosis using amiloride (40 μM). **(G)** Inhibition of phagocytosis using cytochalasin B (2 μM). Mean values ± standard deviation were obtained from three independent experiments. One-way ANOVA, followed by Tukey's post-analysis test were used to determine statistical significance of the data obtained using different inhibitors, compared with the cells treated with PNFs only (**$p < 0.01$; ***$p < 0.005$).
MFI: Mean fluorescence intensity; PNF: Peptide nanofiber.

In vitro effects of PNF:siRNA complexes

Gene silencing induced by PNF:siPLK1 complexes

The biological activity of PNF:si*PLK1* complexes was firstly assessed by delivering si*PLK1 in vitro* to U-87 MG-Luc2 cells. Effects on gene down regulation and protein expression were assessed using RT-qPCR and

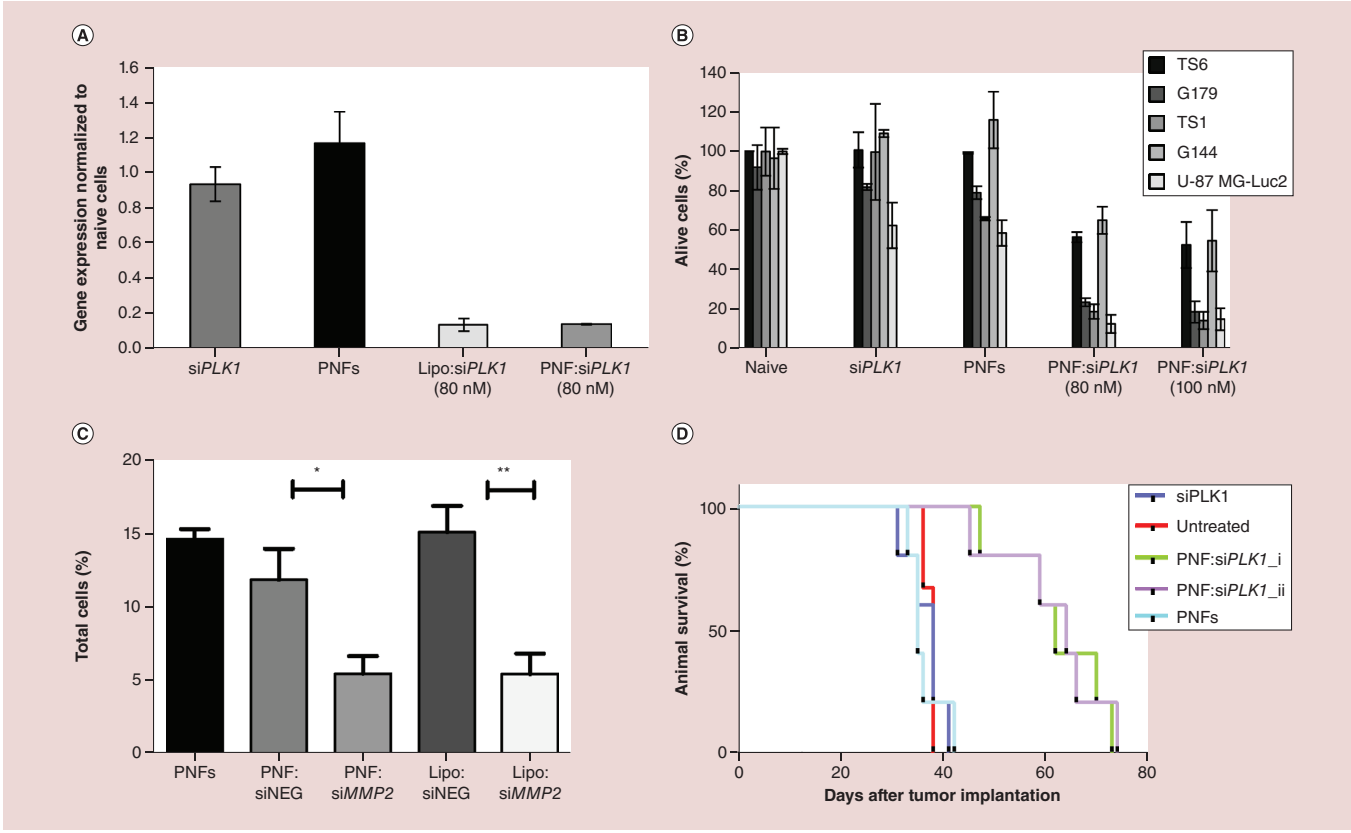

Figure 6. Effect of peptide nanofiber siRNA *in vitro* and *in vivo*. (A) *In vitro* gene silencing analyzed after 24 h of treatment with PNF:si*PLK1* by RT-qPCR. *PLK1* gene expression was normalized using GADPH. Data are averaged of n = 3 and error bars represent standard deviation (one-way ANOVA, $p < 0.0001$). **(B)** Cell viability of a panel of glioblastoma derived stem cells (TS6, G179, TS1 and G144) and glioblastoma immortalized U-87 MG-Luc2 cells was assessed 24 h after treatment with PNF:si*PLK1* complexes (80 and 100 nM). si*PLK1* only and PNFs only were used as negative control treatments. Cells were harvested and cell count was performed using the Scepter™ Cell Counter. **(C)** Cell invasion assay. Cells were treated with PNF:si*MMP2*, PNF:siNEG, Lipofectamine:si*MMP2*, Lipofectamine:siNEG or PNFs only. Statistical significance was analyzed using unpaired t-test, *$p < 0.05$, **$p < 0.01$, n = 5. **(D)** Kaplan–Meier analysis of the survival of tumor-bearing mice treated with PNF:si*PLK1* complexes (n = 5) receiving one (PNF:siGA*PLK1*_i) or two rounds of treatment (PNF:si*PLK1*_ii) and of untreated (n = 4), animals treated with si*PLK1* only (n = 5) and PNFs vector only (n = 5).
PNF: Peptide nanofiber.

immunofluorescence. 24 h after transfection of the cells with PNF:si*PLK1* complexes, *PLK1* mRNA levels were significantly lower for the cells treated with the PNF:si*PLK1* constructs, as shown with RT-qPCR analysis, in comparison with controls of si*PLK1* and PNFs only treated cells (Figure 6A) indicating that PNFs were able to intracellularly deliver biologically active si*PLK1* molecule. The ability of the PNF:si*PLK1* construct to exert their therapeutic effect was furthermore assessed *in vitro* by looking at the expression of PLK1 protein, using immunofluorescence. U-87 MG-Luc2 cells were transfected with PNF:si*PLK1* complexes for 4 h and the levels of the expression of PLK1 protein were observed 24 h after treatment by immunofluorescence. As expected, cells transfected with the PNF:si*PLK1* complexes were showing decreased immunofluorescence signal in comparison with untreated cells and control cells treated with si*PLK1* and siNEG only, PNFs:siNEG and PNFs alone (Supplementary Figure 1A).

Cell death induced by PLK1 silencing using PNF:siPLK1 complexes

Effect of si*PLK1* on the cellular level translates through downregulation of *PLK1* gene expression leading to the mitotic arrest and subsequent cell death. In order to assess cell death induced by PNF:si*PLK1* complexes, cells were transfected using noncytotoxic concentration of PNFs (8 μg/ml), as shown by the LDH cytotoxicity assay in Supplementary Figure 1B. Release of the cytoplasmic LDH as a result of cell membrane damage caused by the PNFs was significantly high only at doses above 25 μg/ml. Cell death induced by silencing of *PLK1* was also evaluated

by measuring cell viability 24 h after treatment of U-87 MG-Luc2 and a panel of cancer stem cells derived from biopsies (Figure 6B) using a semi-automated Scepter Counter™. These data suggest that PLK1 protein knockdown was causing decreased cell viability not only in immortalized tumor cells (U-87 MG-Luc2) but also in a variety of biopsy-derived tumor cell lines: glioblastoma-derived neural stem cells (TS6, TS1, G179 and G144).

Inhibition of cellular migration induced by MMP2 silencing using PNF:siMMP2 complexes

To further evaluate the ability of PNFs to act as intracellular transporters of biologically active siRNA molecules, we also studied the effect of silencing of *MMP2* (playing crucial role in the migration of the cells) on the invasion capability of U-87 MG cells using Cell Invasion Assay (Figure 6C & Supplementary Figure 2). As shown in Figure 6C & Supplementary Figure 2, the invasion of U-87 MG cells was significantly impaired after treatment with PNF:si*MMP2* and the Lipofectamine:si*MMP2* (used as a positive control) comparing with the treatment with Lipo:siNEG, PNF:siNEG and PNF only used as negative controls.

In vivo therapeutic efficacy of PNF:si*PLK1* complexes in GBM-bearing mice.

To generate an orthotopic GBM model, we stereotactically injected 2×10^5 of U-87 MG-Luc2 cells in the right striatum of athymic nude (Foxn1nu/Foxn1+) mice (Supplementary Figure 3A). To assess tumor engraftment, location and growth, three animals per group were subcutaneously administered with D-luciferin. The arising bioluminescent signal was expressed as Total Flux in photons/seconds (Supplementary Figure 3A). The generated xenograft orthotropic GBM model was used to assess therapeutic efficacy of locally administered PNF:si*PLK1* compared with controls of PNFs only and si*PLK1* only in treated and untreated mice. Animals (n = 4–5) were stereotactically injected with the treatments 14 days after tumor implantation, with only one group of animals receiving a second administration of PNF:si*PLK1* (PNF:si*PLK1*_ii) 21 days after tumor implantation. Tumor growth in control animal groups increased rapidly (Supplementary Figure 3B), while the growth rate in animals that received the local administration of PNF:si*PLK1* complexes was slower, indicating that the si*PLK1* delivery mediated by the PNF vectors at cellular level was achieving therapeutic efficacy and slowing down the tumor growth. According to the Kaplan–Meier survival analysis (Figure 6D), mice administered with si*PLK1* only had a median survival of 38 days, similarly to the untreated mice. As shown in Figure 6D, mice treated with PNF vector only had a median survival of 35 days. Interestingly, mice locally administered with the PNF:si*PLK1* complexes showed an improved median survival of 62 days. Second administration of PNF:si*PLK1* complexes was not found to significantly improve the overall survival, as the median survival was 64 days (Figure 6D).

Discussion

The major hurdle in translating siRNA-based therapeutics into the clinic is their poor delivery efficiency. This is particularly problematic in the case of delivery to the CNS, as the presence of blood–brain barrier limits the entrance of exogenous substances to the brain [34,35]. Another problem for delivery of molecules with therapeutic potential, such as siRNA, is their poor penetration across cell membranes. Complexation of siRNA molecules with delivery carriers of different chemical composition has become a standard approach to protect therapeutic siRNA from degradation and enable it to reach its target. Along with that, an important aspect is to minimize the risks of off targeting and side effects, while at the same time achieving an effective delivery at the tumor site. Numerous nanomedicine-based platforms have been designed to address these issues [36–40].

Here, we propose a method of intervention that builds on our previously reported technology of brain localized delivery system [11,12], combined to a *PLK1* gene, involved in cell division [16]. Tumor heterogeneity is one of the major challenges for the development of therapeutics for successful treatment of GBM [36,37]. For this reason, we selected *PLK1* as therapeutic target, a specific gene that is involved in cell division both in biopsy derived cancer stem cells [22] and in U-87 MG cells. PNF:si*PLK1* complexes can be used as a nano-neurosurgical tool following resection of the primary tumor to complement the therapy, as it will aim to prevent further tumor progression. Indeed, tumor progression appears in the wall of resection cavity or within 2 cm from its margin in about half of the patients undergoing brain tumor surgical resection [41]. In contrast to systemic administration, localized intervention will also have the advantage to concentrate the therapy at the tumor site, bypassing the blood–brain barrier, but also to minimize off-target effects often linked to systemically administered RNAi therapy delivery.

Lipid-based nanoparticles that achieve good transfection efficiency *in vitro* are mainly taken-up by the cells via endocytosis and rely mostly on proton-sponge effect or membrane fusion to release their nucleic acid cargo from the endosomal compartments into the cytosol [42,43]. We aimed to understand whether PNFs were able to enter the cells

through passive diffusion across plasma membrane and deliver siRNA directly into the cytosol, therefore, offering advantage in siRNA delivery comparing with conventionally used lipid-based nanoparticles. Subcellular localization of PNF:siRNA complexes was qualitatively and semi-quantitatively assessed using confocal microscopy and imaging flow cytometry. This approach has already been used to accurately assess the uptake of a variety of nanomaterials [30–32,44]. The results of our internalization studies consistently demonstrate that even in energy-depleted conditions, a small fraction of PNFs localizes inside cancer cells (Figures 1B & 2C), in higher percentage in comparison with phagocytic cells such as BV-2 (Figure 3C). The specific inhibition of cell uptake pathways (Figures 4 & 5) also highlights that PNFs can access cytosol by taking advantage of more than one entry route. The ability of PNFs to enter the cells both via energy-dependent and energy-independent pathways can offer more than one option to escape endosomal entrapment and release biologically active siRNA directly in the cytoplasm. Moreover, our data suggest that the uptake of PNFs occurs very early on (30 min) after exposing the cells to these materials. We already demonstrated that PNF:siBcl-2 complexes were capable to outcompete conventional transfecting agents in delivering intracellularly si*Bcl-2* and subsequently inducing cell death in SH-SYSY5 cell line [12]. We hypothesized that the observed difference is due to active as well as passive uptake of PNF:siRNA complexes. In the present work, performed in glioblastoma relevant cell lines, we show that this mechanism is indeed involved in the internalization of PNF:siRNA complexes. Moreover, the biological activity of delivered siRNA molecules was also confirmed in U-87 MG cells using different siRNA molecules. The ability of PNF:siRNA to act as an intracellular carrier of biologically active siRNA in glioblastoma cells was demonstrated on *PLK1* mRNA and protein levels, but also in downstream cellular effect, by eliciting cell death. PNFs potential to deliver biologically active siRNA molecules is also supported by the results obtained after silencing the expression of *MMP2* gene (Supplementary Figure 4), which led to preventing tumor migration. Delivering combined siRNAs, such as *PLK1* and *MMP2*, targeting oncogenes relevant for glioblastoma therapy is also an avenue that could be explored, as it has been reported that multiplexed RNAi therapies targeting brain initiating tumor cells can slow down tumor growth [37].

At last, as a proof of concept, we evaluated the effect of PNF:si*PLK1* complexes *in vivo*. Our data indicate that intratumoral injection of PNF:si*PLK1* offers a considerable benefit in comparison with the siRNA control injected animals by effectively doubling the survival median proportion, while second administration 1 week after the first administration did not further ameliorate the prognosis. One possible explanation is limited travelling of PNFs from the site of injection to the periphery of the tumor. Further studies are required to fully understand the way PNF:siRNA complexes interact with tumor cells *in vivo*. It has already been shown that the chemistry of the nanoparticles and the use of an osmotic pump for convection-enhanced delivery can considerably increase the ability of nanoparticles to spread within the brain parenchyma at distal sites from the area of infusion [45,46]. Coupling this therapy to convection-enhanced delivery may offer additional survival as it could help to overcome the limited benefit obtained with the bolus injection.

Conclusion

We have demonstrated the capacity of PNFs to act as a delivery platform for siRNA molecules *in vitro*. Selective inhibition of main endocytic pathways demonstrated that PNFs could enter the cells via all major internalization pathways, but more importantly via passive translocation across plasma membrane representing a promising tool for direct cytosolic delivery of siRNA molecules. The PNF:siRNA complexes were found to efficiently deliver biologically active siRNA molecules (targeting *PLK1* and *MMP2* genes) affecting cell viability and migration capacity in a panel of cancer cells. Finally, we demonstrated that PNF:si*PLK1* complexes can potentially be exploited as a new nano-neurosurgical tool *in vivo* and be further investigated as adjunctive therapy administered locally upon resection of the primary tumor in an effort to avoid tumor progression from the resection margins and facilitate translation of RNAi therapeutics for the benefit of GBM patients.

Future perspective

Further studies should focus on understanding how PNF:siRNA complexes interact with tumor cells *in vivo*. More specifically, it is important to assess the distribution of PNF:siRNA complexes upon intratumoral injection as well as the diffusion capacity of the complexes. Gene silencing *in vivo* could also be assessed as part of the future work.

Supplementary data

To view the supplementary data that accompany this paper please visit the journal website at www.futuremedicine.com/doi/suppl/10.2217/nnm-2019-0298

Acknowledgments

The authors would like to acknowledge H Bradley and A Banyard for technical help and fruitful discussions, CRUK funded Imagestream Facility, Manchester Collaborative Centre for Inflammation Research (MCCIR) funded Single Cell Facility as well as Bioimaging Facility in the University of Manchester.

Financial & competing interests disclosure

This work was partially funded by the University of Manchester and by 'RADDEL' Marie Curie Initial Training Network (ITN) grant under the EU's FP7 PEOPLE program. The authors have no other relevant affiliations or financial involvement with any organization or entity with a financial interest in or financial conflict with the subject matter or materials discussed in the manuscript apart from those disclosed.

No writing assistance was utilized in the production of this manuscript.

Summary points

- The uptake mechanism of peptide nanofibers (PNFs) was studied in two cell types (U-87 MG and BV-2) representative of glioblastoma multiforme, using confocal microscopy, flow cytometry and imaging flow cytometry.
- Using inhibitors of endocytosis, we show that PNFs enter the cells via passive as well as active mechanisms.
- PNFs were able to deliver siRNA that silenced *PLK1* and *MMP2* genes leading to cell death or impaired migratory capacity of U-87 MG cells, respectively.
- Intratumoral injection of PNF:si*PLK1 in vivo* led to significantly longer survival time of tumor bearing animals.

References

Papers of special note have been highlighted as: • of interest; •• of considerable interest

1. Kircher MF, de la Zerda A, Jokerst JV *et al.* A brain tumor molecular imaging strategy using a new triple-modality MRI-photoacoustic-Raman nanoparticle. *Nat. Med.* 18(5), 829–834 (2012).
2. Stupp R, Mason WP, van den Bent MJ *et al.* Radiotherapy plus concomitant and adjuvant temozolomide for glioblastoma. *N. Engl. J. Med.* 352(10), 987–996 (2005).
3. Alphandéry E. Glioblastoma treatments: an account of recent industrial developments. *Front. Pharmacol.* 9, 879 (2018).
4. Weller M, Cloughesy T, Perry JR, Wick W. Standards of care for treatment of recurrent glioblastoma – are we there yet? *Neuro. Oncol.* 15(1), 4–27 (2013).
5. Gavrilov K, Saltzman WM. Therapeutic siRNA: principles, challenges, and strategies. *Yale J. Biol. Med.* 85(2), 187–200 (2012).
6. Ryther RC, Flynt AS, Phillips JA, Patton JG. siRNA therapeutics: big potential from small RNAs. *Gene Ther.* 12(1), 5–11 (2005).
7. Zuckerman JE, Davis ME. Clinical experiences with systemically administered siRNA-based therapeutics in cancer. *Nat. Rev. Drug Discov.* 14(12), 843–856 (2015).
8. Tatiparti K, Sau S, Kashaw SK, Iyer AK. siRNA delivery strategies: acomprehensive review of recent developments. *Nanomaterial* 7(4), 77 (2017).
9. Malhotra M, Toulouse A, Godinho BM, McCarthy DJ, Cryan JF, O'Driscoll CM. RNAi therapeutics for brain cancer: current advancements in RNAi delivery strategies. *Mol. Biosyst.* 11(10), 2635–2657 (2015).
10. Chakroun RW, Zhang P, Lin R, Schiapparelli P, Quinones-Hinojosa A, Cui H. Nanotherapeutic systems for local treatment of brain tumors. *WIREs Nanomed. Nanobiotechnol.* 10(1), e1479 (2018).
11. Mazza M, Patel A, Pons R, Bussy C, Kostarelos K. Peptide nanofibres as molecular transporters: from self-assembly to *in vivo* degradation. *Faraday Discuss.* 166, 181–194 (2013).

•• **Description and characterization of peptide nanofibers used in this study.**

12. Mazza M, Hadjidemetriou M, De Lázaro I, Bussy C, Kostarelos K. Peptide nanofiber complexes with siRNA for deep brain gene silencing by stereotactic neurosurgery. *ACS Nano* 9(2), 1137–1149 (2015).

•• **Description and characterization of peptide nanofibers used in this study.**

13. Zhang P, Cheetham AG, Lin YA, Cui H. Self-assembled Tat nanofibers as effective drug carrier and transporter. *ACS Nano* 7(7), 5965–5977 (2013).
14. Soukasene S, Toft DJ, Moyer TJ *et al.* Antitumor activity of peptide amphiphile nanofiber-encapsulated camptothecin. *ACS Nano* 5(11), 9113–9121 (2011).
15. Kalafatovic D, Nobis M, Son J, Anderson KI, Ulijn RV. MMP-9 triggered self-assembly of doxorubicin nanofiber depots halts tumor growth. *Biomaterials* 98, 192–202 (2016).

16. Barr FA, Silljé HH, Nigg EA. Polo-like kinases and the orchestration of cell division. *Nat. Rev. Mol. Cell Biol.* 5(6), 429–440 (2004).
17. Takai N, Hamanaka R, Yoshimatsu J, Miyakawa I. Polo-like kinases (Plks) and cancer. *Oncogene* 24(2), 287–291 (2005).
18. Mikheeva SA, Mikheev AM, Petit A *et al.* TWIST1 promotes invasion through mesenchymal change in human glioblastoma. *Mol. Cancer* 9, 18 (2010).
19. Pezuk JA, Brassesco MS, Morales AG *et al.* Polo-like kinase 1 inhibition causes decreased proliferation by cell cycle arrest, leading to cell death in glioblastoma. *Cancer Gene Ther.* 20(9), 499–506 (2013).
20. Lénárt P, Petronczki M, Steegmaier M *et al.* The small-molecule inhibitor BI 2536 reveals novel insights into mitotic roles of polo-like kinase 1. *Curr. Biol.* 17(4), 304–315 (2007).
21. Steegmaier M, Hoffmann M, Baum A *et al.* BI 2536, a potent and selective inhibitor of polo-like kinase 1, inhibits tumor growth *in vivo*. *Curr. Biol.* 17(4), 316–322 (2007).
22. Danovi D, Folarin A, Gogolok S *et al.* A high-content small molecule screen identifies sensitivity of glioblastoma stem cells to inhibition of polo-like kinase 1. *PLoS ONE* 8(10), e77053 (2013).
23. Gorlick R, Kolb EA, Keir ST *et al.* Initial testing (stage 1) of the polo-like kinase inhibitor volasertib (BI 6727), by the pediatric preclinical testing program. *Pediatr. Blood Cancer* 61(1), 158–164 (2014).
24. Tandle AT, Kramp T, Kil WJ *et al.* Inhibition of polo-like kinase 1 in glioblastoma multiforme induces mitotic catastrophe and enhances radiosensitisation. *Eur. J. Cancer* 49(14), 3020–3028 (2013).
25. Schöffski P, Blay JY, De Greve J *et al.* Multicentric parallel Phase II trial of the polo-like kinase 1 inhibitor BI 2536 in patients with advanced head and neck cancer, breast cancer, ovarian cancer, soft tissue sarcoma and melanoma. The first protocol of the European Organization for Research and Treatment of Cancer (EORTC) Network Of Core Institutes (NOCI). *Eur. J. Cancer* 46(12), 2206–2215 (2010).
26. Sebastian M, Reck M, Waller CF *et al.* The efficacy and safety of BI 2536, a novel Plk-1 inhibitor, in patients with stage IIIB/IV non-small cell lung cancer who had relapsed after, or failed, chemotherapy: results from an open-label, randomized Phase II clinical trial. *J. Thorac. Oncol.* 5(7), 1060–1067 (2010).
27. Lee C, Fotovati A, Triscott J *et al.* Polo-like kinase 1 inhibition kills glioblastoma multiforme brain tumor cells in part through loss of SOX2 and delays tumor progression in mice. *Stem Cells* 30(6), 1064–1075 (2012).
28. Lerner RG, Grossauer S, Kadkhodaei B *et al.* Targeting a Plk1-controlled polarity checkpoint in therapy-resistant glioblastoma-propagating cells. *Cancer Res.* 75(24), 5355–5366 (2015).
29. Pollard SM, Yoshikawa K, Clarke ID *et al.* Glioma stem cell lines expanded in adherent culture have tumor-specific phenotypes and are suitable for chemical and genetic screens. *Cell Stem Cell* 4(6), 568–580 (2009).
30. Vranic S, Boggetto N, Contremoulins V *et al.* Deciphering the mechanisms of cellular uptake of engineered nanoparticles by accurate evaluation of internalization using imaging flow cytometry. *Part. Fibre Toxicol.* 10, 2 (2013).
31. Vranic S, Gosens I, Jacobsen NR *et al.* Impact of serum as a dispersion agent for *in vitro* and *in vivo* toxicological assessments of TiO_2 nanoparticles. *Arch. Toxicol.* 91(1), 353–364 (2016).
32. Martincic M, Vranic S, Pach E *et al.* Non-cytotoxic carbon nanocapsules synthesized via one-pot filling and end-closing of multi-walled carbon nanotubes. *Carbon* 141, 782–793 (2019).
33. Guo C, Al-Jamal WT, Toma FM *et al.* Design of cationic multiwalled carbon nanotubes as efficient siRNA vectors for lung cancer xenograft eradication. *Bioconjug. Chem.* 26(7), 1370–1379 (2015).

- **Use of carbon nanotubes as siRNA delivery vectors.**

34. Pardridge WM. CSF, blood–brain barrier, and brain drug delivery. *Expert Opin. Drug Deliv.* 13(7), 963–975 (2016).
35. Tam VH, Sosa C, Liu R, Yao N, Priestley RD. Nanomedicine as a non-invasive strategy for drug delivery across the blood brain barrier. *Int. J. Pharm.* 515(1–2), 331–342 (2016).
36. Cohen ZR, Ramishetti S, Peshes-Yaloz N *et al.* Localized RNAi therapeutics of chemoresistant grade IV glioma using hyaluronan-grafted lipid-based nanoparticles. *ACS Nano* 9(2), 1581–1591 (2015).
37. Yu D, Khan OF, Suvà ML *et al.* Multiplexed RNAi therapy against brain tumor-initiating cells via lipopolymeric nanoparticle infusion delays glioblastoma progression. *Proc. Natl Acad. Sci. USA* 114(30), E6147–E6156 (2017).
38. Lollo G, Vincent M, Ullio-Gamboa G *et al.* Development of multifunctional lipid nanocapsules for the co-delivery of paclitaxel and CpG-ODN in the treatment of glioblastoma. *Int. J. Pharm.* 495(2), 972–980 (2015).
39. Lee TJ, Haque F, Shu D *et al.* RNA nanoparticle as a vector for targeted siRNA delivery into glioblastoma mouse model. *Oncotarget* 6(17), 14766–14776 (2015).
40. Kozielski KL, Tzeng SY, De Mendoza BA, Green JJ. Bioreducible cationic polymer-based nanoparticles for efficient and environmentally triggered cytoplasmic siRNA delivery to primary human brain cancer cells. *ACS Nano* 8(4), 3232–3241 (2014).
41. Konishi Y, Muragaki Y, Iseki H, Mitsuhashi N, Okada Y. Patterns of intracranial glioblastoma recurrence after aggressive surgical resection and adjuvant management: retrospective analysis of 43 cases. *Neurol. Med. Chir. (Tokyo)* 52(8), 577–586 (2012).

42. Gilleron J, Querbes W, Zeigerer A *et al.* Image-based analysis of lipid nanoparticle-mediated siRNA delivery, intracellular trafficking and endosomal escape. *Nat. Biotechnol.* 31(7), 638–646 (2013).
43. Jhaveri A, Torchilin V. Intracellular delivery of nanocarriers and targeting to subcellular organelles. *Expert Opin. Drug Deliv.* 13(1), 49–70 (2016).
44. Marangon I, Boggetto N, Ménard-Moyon C *et al.* Localization and relative quantification of carbon nanotubes in cells with multispectral imaging flow cytometry. *J. Vis. Exp.* 2013(82), e50566 (2013).
45. Song E, Gaudin A, King AR *et al.* Surface chemistry governs cellular tropism of nanoparticles in the brain. *Nat. Commun.* 8, 15322 (2017).
46. Mastorakos P, Zhang C, Berry S *et al.* Highly PEGylated DNA nanoparticles provide uniform and widespread gene transfer in the brain. *Adv. Healthc. Mater.* 4(7), 1023–1033 (2015).